Functional Integration of Ni-Mo Electrocatalysts with Si Microwire Array Photocathodes to Simultaneously Achieve High Fill Factors and Light-Limited Photocurrent Densities for Solar-Driven Hydrogen Evolution

Matthew R. Shaner[α,β], James R. McKone[α,‡], Harry B. Gray[Ψ,α], and Nathan S. Lewis[Ψ,α,β]

[Ψ]Beckman Institute and Kavli Nanoscience Institute
[α]Division of Chemistry and Chemical Engineering
[β]Joint Center for Artificial Photosynthesis
California Institute of Technology,
1200 East California Blvd, Pasadena, California 91125

E-mail: nslewis@caltech.edu

*To whom correspondence should be addressed

[‡]Current address: Department of Chemistry, Cornell University, Ithaca NY

Abstract

An n^+p-Si microwire array coupled with a two-layer catalyst film consisting of Ni–Mo nanopowder and TiO_2 light-scattering nanoparticles has been used to simultaneously achieve high fill factors and light-limited photocurrent densities from photocathodes that produce $H_2(g)$ directly from sunlight and water. The TiO_2 layer scattered light back into the Si microwire array, while optically obscuring the underlying Ni–Mo catalyst film. In turn, the Ni-Mo film had a mass loading sufficient to produce high catalytic activity, on a geometric area basis, for the hydrogen-evolution reaction. The best-performing microwire devices prepared in this work exhibited short-circuit photocurrent densities of -14.3 mA cm^{-2}, photovoltages of 420 mV, and a fill factor of 0.48 under 1 Sun of simulated solar illumination, whereas the equivalent planar Ni-Mo-coated Si device, without TiO_2 scatterers, exhibited negligible photocurrent due to complete light blocking by the Ni–Mo catalyst layer.

Formatted: Not Highlight

Formatted: Not Highlight

Keywords: Hydrogen evolution; Electrocatalysis; Silicon; Photocathode; Molybdenum; Nickel; Platinum; Ni–Mo nanopowder; Earth-abundant

Broader Context

Solar-driven photoelectrochemical water splitting is a promising approach to enable the large-scale conversion and storage of solar energy. Few integrated systems have been realized that use earth-abundant semiconductor and catalyst materials for the half-reactions involved in solar-driven water-splitting, i.e. hydrogen evolution and oxygen evolution, while also achieving high energy-conversion efficiencies. We describe herein a hydrogen-evolving Si-based photoelectrode that exhibits high light-limited photocurrent densities, as well as high catalytic activities, while using a high mass loading of an earth-abundant electrocatalyst. The design is reminiscent of a membrane-electrode assembly as used for stand-alone fuel cell and electrolysis systems. The approach exploits the high aspect ratio of the absorber layer to avoid parasitic optical absorption normally associated with a thick catalyst layer on the surface of an illuminated photocathode.

I. INTRODUCTION

Photon management is an important attribute of photoelectrodes used for solar-driven water-splitting, especially for device architectures that incorporate optically opaque electrocatalyst

coatings on the surface of a light absorbing material.[1-4] Specifically, the fill factor (*ff*) is generally negatively correlated with the light-limited photocurrent density (J_{ph}), because increases in catalyst loading increase the *ff*, but also produce larger parasitic optical absorption losses and thus decrease the value of J_{ph} (Figure 1).[1] Such behavior is especially apparent for earth-abundant electrocatalysts for the hydrogen-evolution reaction (HER), which are generally optically opaque and require large mass loadings ($\geq$ 1 mg cm^{-2}) to achieve the requisite catalytic activity.[5-7] Similar issues can also preclude optimal functional incorporation of currently available electrocatalysts for the oxygen-evolution reaction (OER) into integrated photoanode structures for the solar-driven oxidation of H_2O to O_2(g).[8,9]

Deleted: Figure 1

For planar photoelectrode architectures, various options to mitigate this deleterious tradeoff between catalytic activity and optical transparency have been developed. For discrete photovoltaic (PV)-biased electrolysis systems[1-4,10], the PV device can be connected electrically to discrete, catalytic electrodes that do not physically obscure incoming light from the PV cell, with the interfacial reactions being performed by majority carriers.[1,11] Alternatively, in photoelectrode structures comprised of a single photoabsorber, a transparent back contact can be used in conjunction with "backside" illumination so that the catalyst layer is not in the optical path of the semiconductor.[5-7,12] For integrated photoelectrodes in which the interfacial reactions can be performed by photogenerated minority carriers (as well as by majority carriers, for structures that contain a buried junction[8-10]), the thickness of the electrocatalyst film can be adjusted to obtain an optimum compromise between the optical density and activity of the electrocatalyst film. This type of optimization favors the use of an extremely thin (< 5 nm) catalytic layer, at the expense of catalytic activity.[9] In certain instances, nanostructuring can produce optically transparent, highly active films of noble metal electrocatalysts.[4] Yet another method involves optimization of the spatial location and areal coverage of islands of an active, but optically absorbing electrocatalyst film, by use of a photolithographic or shadow mask.[13] This approach is analogous to the use of grid-line top contacts in photovoltaics.

Absorbers that are structured in three dimensions, such as Si microwire arrays[14-17] provide an alternative, general approach to ameliorating the negative correlation between the *ff* and J_{ph}. In such systems, a relatively high loading of catalyst can be positioned at the base of a high-aspect-ratio microwire array, leaving exposed a large proportion of the array (Figure 2). For example,

Deleted: Figure 2

earth-abundant metal catalysts such as Ni–Mo[5], Ni or Co phosphide[6,7], or Mo chalcogenides[18] with mass loadings on the order of 1 mg cm^{-2} (i.e. several μm thick) exhibit comparable geometric HER activity to a planar > 10 nm thick Pt film. By comparison, the depth over which light can be completely absorbed in a sparse silicon microwire array with appropriate scattering elements is on the order of 100 μm. The relatively low proportional volume occupied by high catalyst mass loadings can therefore enable high overall catalytic activity while preserving optical accessibility to the majority of the light-absorber material.

A recent study has shown that a CoP HER electrocatalyst could be deposited at the base of a Si microwire array, yielding activity toward photoelectrochemical hydrogen evolution comparable to that of a control sample that instead used Pt as the HER electrocatalyst.[19] Si microwire arrays, however, do not absorb a large proportion of incoming, normally incident photons on the "first pass" of such photons through the structure of the device.[8] As a result, significant parasitic optical absorption occurs in such devices even with the catalyst film deposited exclusively at the base of the array. An improved device structure, which we denote as the "MEA" architecture, resembles a fuel cell or to an electrolyzer membrane-electrode assembly (MEA) (Figure 2). Such a structure is characterized by a Si microwire array on the order of 100 μm in height with a 5–10 μm thick porous catalyst layer consisting of an earth-abundant electrocatalyst, such as Ni–Mo, Mo sulfide, or a transition-metal phosphide, in addition to a 1–3 μm thick porous light-scattering layer, such as particulate TiO_2 or another high-dielectric scattering material. The catalyst layer is analogous to the one found in a conventional MEA, whereas the light-scattering layer serves as an optical scattering element as well as a gas-diffusion layer. The microwires act as current collectors by absorbing solar photons and producing sufficient electrochemical potential to effect the HER.

Deleted: Figure 2

In this approach, if the catalyst and scattering layers are both sufficiently porous, reactant species (e.g., water or H^+) can diffuse through and hydrogen gas can diffuse out of the internal volume of the device. However, when incident on the scattering layer, photons will be reflected laterally and will therefore pass multiple times through the Si microwires. An analogous light-scattering design was proposed and validated for Si microwire photovoltaics, and high light-limited photocurrent densities (> 15 mA cm^{-2} at 100 mW cm^{-2} of Air Mass (AM) 1.5G simulated illumination intensity) were indeed obtained in that system.[8,20] In principle, the MEA approach

allows for simultaneous maximization of the catalytic activity and optical absorption in the semiconducting material, even when a relatively large mass loading of electrocatalyst is required. In this work, we have modeled and validated the MEA design using Si microwire-array photocathodes to drive the HER in conjunction with a Ni–Mo nanopowder catalyst and a TiO_2 light-scattering layer.

II. MODELING AND EXPERIMENTAL

A brief summary of the modeling and experimental details are provided below, with additional details included in the Supplementary Information.

Modeling

A zero-dimensional model was constructed to predict the maximum performance expected from the MEA-type photocathode device, based on a previously derived analytical expression for a buried junction in series with a catalyst and an additional resistor.[21] Two-dimensional full-wave electromagnetic simulations were used to determine the light-limited current density of the microwire structure, to provide input into the device model. The catalytic performance was determined by modeling experimental data using the Butler-Volmer equation and by incorporation of a series resistance as determined experimentally by impedance measurements.

Experimental

Si (p-type) microwires were grown in a custom-built chemical-vapor deposition (CVD) reactor via a vapor-solid-liquid process.[22] The growth wafers were patterned with 3 μm diameter Cu catalysts located via photolithography in square pattern with a 7 μm pitch. Highly doped n^+-Si emitters were formed by use of a phosphorous-doped spin-on-glass.

Ni-Mo nanopowder was synthesized following a previously reported procedure.[5] A Ni-Mo catalyst supported on carbon (Ni-Mo/C) was synthesized similarly to the Ni-Mo nanopowder except for use of an additional step that involved thoroughly grinding the Ni-Mo oxide with carbon black to form the supported structure. TiO_2 and Ni-Mo nanopowders were suspended in isopropanol at concentrations of 100 mg mL^{-1} and 1-2 mg mL^{-1}, respectively. The Ni-Mo nanopowder was deposited onto Ti foil electrodes or onto Si photoelectrodes (both planar and microwire arrays) by centrifugal flocculation from the nanoparticle inks, to achieve mass loadings

of ~1 mg cm^{-2}. The Ni-Mo, but not Ni-Mo/C catalysts, were actived after deposition by an anneal at 450 °C in forming gas. 15 μL of the TiO_2 nanopowder solution was deposited in a nominally identical fashion to that used to deposit Ni-Mo nanopowders onto Si samples. Platinum catalysts, used for control experiments, were deposited electrolessly on Si substrates by use of a solution that consisted of 1 mM Pt and 2% HF in H_2O.

Hydrogen-saturated, trace-metal-grade sulfuric acid (0.5 or 1.0 M) solutions were used to determine the cyclic voltammetric performance of the electrodes using a three-electrode electrochemical configuration. The electrolyte was constantly bubbled with research grade $H_2(g)$ (AirLiquide) to maintain a constant reversible hydrogen electrode (RHE) potential, as determined by measurement of the open-circuit potential of an electrochemically cleaned Pt button electrode. Simulated 1-Sun illumination was provided by an ELH-type tungsten-halogen lamp or by a Xe lamp with an AM 1.5G filter. Spectral response measurements with the electrodes maintained potentiostatically -0.15 V versus the reversible hydrogen electrode, RHE, were performed with a custom-built apparatus under electrochemical testing conditions that were nominally identical with those used for collection of the cyclic voltammetric data.

III. RESULTS

Figure 3 shows the modeling results (see Supplementary Information for details of the model parameters) for a photocathode consisting of an n^+p-Si microwire array in conjunction with a Ni–Mo nanopowder catalyst covered by a porous TiO_2 light-scattering overlayer. To provide a first-order approximation to the maximum expected device performance for such a structure, the modeling treated the integrated photoelectrode as a zero-dimensional, series-connected n^+p-Si junction coupled to a catalyst layer and to a resistive circuit element. The increased dark-current junction area (γ in Equation S1), and the series resistance required to transport electrons down the length of the microwire through the n^+-Si emitter to the catalyst, were considered explicitly. The light-limited current density was obtained through two-dimensional full-wave electromagnetic simulations of a Si microwire array architecture.[3,4] The modeling indicated that utilization of a stand-alone n^+p-Si microwire array PV device having a solar energy-conversion efficiency of 12.9% could, in principle, yield a maximum ideal regenerative cell efficiency (η_{IRC})[23] of 11.2% based on the hydrogen-evolution half-reaction being performed at such a photocathode. This value

Deleted: Figure 3

is essentially the same as the value that would be obtained by wiring the respective photovoltaic device to a discrete, catalytic electrode obtained by using a high mass-loading of the Ni–Mo HER catalyst on an inert conducting substrate.

Figure 4a,b shows a scanning-electron micrograph of a Si microwire array coated at the base by a layer of Ni–Mo nanopowder, with the Si and Ni–Mo bound together by a small quantity of poly-tetrafluoroethylene (PTFE). The structure also contained an overlayer of TiO_2 nanoparticles bound together with a Nafion ionomer, in accord with the full device structure depicted schematically in Figure 2.[24] Figure 4b has been highlighted to delineate the layers of Ni–Mo and TiO_2, respectively, and clearly demonstrates the successful fabrication of the desired MEA photocathode structure. Figure 4c shows an optical image of four microwire samples. A bare Si microwire array was iridescent and reflective, similar to the starting wafer prior to microwire growth, because of the highly ordered, sparse microwire array. However, the addition of a Ni-Mo catalyst layer altered the appearance to a matte black, due to the optical absorption in both the microwires and the Ni-Mo electrocatalyst. Deposition of a nanoparticulate TiO_2 layer directly onto the base of the Si microwire array, or over a Ni–Mo film, yielded a gray photoelectrode, consistent with scattering of a large proportion of the incoming light into the vertically oriented Si microwires. The sample that contained an underlying Ni-Mo layer was slightly darker, due to imperfect Ni-Mo deposition leaving some residual optically absorbing catalyst on the sidewalls of the microwires.

Figure 5 shows the *J-E* behavior for dark HER electrocatalysis by Ni–Mo nanopowders deposited on planar Ti substrates, as well as for Ni-Mo nanopowders deposited at the bases of degenerately doped p-type Si microwire arrays (p^+-Si MWs), with and without overlayers of TiO_2 particles, respectively. Before catalyst deposition, the Si microwire arrays were metallized with Ag and were annealed to minimize any effects of interfacial contact resistance with the catalyst materials. As indicated in Figure 5, the dark catalytic HER performance of the Ni–Mo films on the Si microwires matched, or slightly exceeded, that exhibited by the same loading of pure Ni–Mo nanopowder on planar Ti electrodes.

Figure 6 depicts the *J-E* behavior observed for illuminated planar Si n^+p-junction photoelectrodes coated with a Ni–Mo/TiO_2 MEA composite film. For Ni-Mo catalyst mass loadings on the order of 1 mg cm^{-2}, the catalyst and scattering film produced nearly complete

Deleted: Figure 4

Deleted: Figure 4

Deleted: Figure 4

Deleted: Figure 5

Deleted: Figure 5

Deleted: Figure 6

blocking of the incident light. For example, with the MEA layers present, the planar n^+p-Si device produced $|J_{ph}| < 1$ mA cm^{-2}, as compared to $|J_{ph}| > 25$ mA cm^{-2} for low loadings of Pt on planar n^+p-Si photocathodes.[25] Increasing the light intensity to ~10 Suns resulted in $J_{ph} \approx -7.5$ mA cm^{-2}, accompanied by a rapid onset of cathodic photocurrent, attesting to the high activity of the Ni–Mo catalyst. Similar results were obtained for Ni–Mo films alone on planar Si substrates, attesting to the extremely high optical opacity of a μm-thick, nanostructured, metallic Ni-Mo catalyst film.

Figure 7 presents the *J-E* behavior of the best-performing Si n^+p-junction microwire array devices prepared in this work that also contained electrocatalyst and/or scattering composites. To investigate the maximum light-limited current density generated solely by the n^+p-Si microwires, a TiO_2 scattering layer was introduced at the base of such a microwire array, to remove any influence from the growth substrate and to increase the length of the optical path through the microwires. Without a catalyst, the light-limited current densities for such a structure approached 25 mA cm^{-2}, in agreement with two-dimensional full-wave modeling simulations. However, illuminated Si microwire arrays without an electrocatalyst exhibited negligible photocurrent density at potentials positive of 0 V vs RHE. In contrast to the behavior without a catalyst, deposition of 2 mg-cm^{-2} of Ni–Mo at the base of the microwire array produced similar J_{ph} values and fill factors to those observed when Pt was electrolessly deposited on the microwire sidewalls (Figure 7).

Table 1 presents the compiled results for photoelectrodes of each type, and Figure S7 presents SEM images each type of device. The best-performing MEA-type device incorporating the Ni–Mo HER catalyst exhibited $V_{oc} = 0.42$ V, $J_{sc} = -14.3$ mA cm^{-2} and a fill factor, $ff = 0.48$, resulting in $\eta_{IRC} = 2.9\%$, without any corrections for solution or mass-transport losses. This efficiency value exceeds previous values of $\eta_{IRC} = 2.2\%$ produced by electrodeposition of Ni–Mo onto Si n^+p-junction microwires.[1,11] For comparison, a device with a TiO_2 scattering layer and a Pt catalyst electrolessly deposited on the sidewalls of the microwires produced $V_{oc} = 0.51$ V, $J_{sc} = -20.2$ mA cm^{-2} and $ff = 0.49$, resulting in $\eta_{IRC} = 5.0\%$. Performance statistics are given in Table S1 for MEA-type device electrodes along with n^+p-Si/Pt planar electrodes.

Figure 8 shows the spectral response data for the best-performing Ni–Mo/TiO_2 and Pt/TiO_2 devices. Integration of the spectral response data with the AM 1.5G spectrum produced light-limited photocurrent densities of 15.8 and 17.5 mA cm^{-2} for the Ni-Mo/TiO_2 and Pt/TiO_2 devices, respectively. These values reflect the trend observed in the *J-E* behavior of each device (c.f. Figure

Deleted: Figure 7
Formatted: Not Highlight
Formatted: Not Highlight
Deleted: Figure 7
Deleted: Table 1
Formatted: Not Highlight
Deleted: Figure 8
Formatted: Not Highlight

7). Consistent with previous reports[9,25], the maximum external quantum yield for the Pt-deposited sample was ~0.6 at ~540 nm, with a monotonic decrease at longer wavelengths.

Diminished photovoltages were generally observed for Si/Ni–Mo MEA devices that had been treated under reducing atmosphere at moderate temperatures (450 °C), relative to Pt-coated samples that had not been annealed. To address this disparity, a modified Ni–Mo nanopowder synthesis was developed involving reduction of the Ni–Mo oxide intermediate powder in the presence of carbon black. This carbon-containing catalyst (Ni–Mo/C) did not require an annealing step after deposition onto Si substrates. Figure 9 compares the *J–E* behavior for n^+p-Si microwire-array photocathodes loaded with the standard Ni–Mo and Ni–Mo/C catalysts, with the latter samples not annealed after deposition of the catalyst layer. These data demonstrate a recovery of the V_{oc} upon removal of the catalyst-activation annealing step.

IV. DISCUSSION

Model: The modeling indicated the performance advantages provided, in principle, by the MEA architecture relative to many other designs for integrated photoelectrodes that contain earth-abundant electrocatalysts. Specifically, the modeling predicts that η_{IRC} >10% is possible (Figure 3), with the main contribution to higher η_{IRC} being provided by the decoupling of the optical absorption and catalytic activity of the electrocatalyst, allowing for simultaneous achievement of high *ff* and J_{ph} values. These predicted efficiencies rival the best-performing previously reported devices for hydrogen-evolving photocathodes that involve noble-metal catalysts.[12,26]

Performance of Ni–Mo Nanopowder Electrocatalysts: Realization of the predicted high η_{IRC} values requires fabrication of high-performance individual components, along with synergistic integration to form full MEA device architectures. One crucial component is the hydrogen-evolution catalyst. Ni-Mo nanopowders have exhibited high activity using a Ni–Mo nanopowder catalyst on planar Ti substrates (Figure 5), yielding overpotentials of -80 mV to produce current densities of -10 mA cm^{-2} for H_2(g) production in 1.0 M H_2SO_4.[5,14-17] As shown in Figure 5, this performance was matched in the MEA structure with Ni–Mo/TiO_2 layers at the base of the metallized Si microwire array. Furthermore, the catalytic activity observed for Ni–Mo even when deposited at the base of a Si microwire array indicated that mass transport of reactants and products was not significantly attenuated by the presence of the microwires or by the porous TiO_2 scattering

Deleted: Figure 7

Deleted: Figure 9

Deleted: Figure 3

Formatted: Not Highlight

Deleted: Figure 5

Deleted: Figure 5

layer.[27] The data also illustrate that Ni–Mo/TiO_2 MEA composite electrodes can be characterized in strongly acidic solutions, due to the high activity and relatively stable initial performance of Ni–Mo nanopowders under such conditions.[5] We note, however, that Ni–Mo nanopowders produced in this way do not exhibit indefinite stability under acidic conditions.

Photoelectrode results: The other main components of the MEA photocathode are the absorber and photovoltage-producing junction, both of which are provided by the n^+p Si microwire array. The observed η_{IRC} = 5% from photoelectrodes formed using thin Pt electrocatalyst layers indicated the formation of high-quality homojunctions in the Si microwires, with high accompanying optical absorption in the material (Figure 7). This combined behavior thus produced similar performance to the best-performing microwire-array photocathodes that have been reported previously.[6,7,25] Integration of the Ni–Mo and TiO_2 layers, to form the complete MEA device depicted in Figure 2, resulted in a η_{IRC} = 2.9% for the best-performing Si microwire photocathodes in conjunction with earth-abundant electrocatalysts that were prepared in this work. This level of performance was obtained by maintaining high catalytic activity and high open-circuit voltages, in conjunction with J_{ph} values 50% larger than those obtained for devices having catalysts deposited on the sidewalls of the microwires.[1,18] Additionally, these devices far outperformed planar devices having similar catalyst loadings, demonstrating the merits of decoupling the catalytic activity with respect to the light-limited current density.

Potential for Improved Device Performance: A comparison between the best-performing device prepared in this work, η_{IRC} = 2.9%, and the predictions of the modeling indicates significant potential for improvement by optimization of the microwire device architecture. The observed V_{oc} and J_{ph} values were markedly lower than those predicted by the idealized, series-connected equivalent-circuit representation of the individual components. Specifically, the best-performing n^+p-Si microwire-array photoelectrodes investigated herein exhibited V_{oc} values between 450 and 550 mV at light intensities sufficient to produce light-limited photocurrent densities of 5–25 mA cm^{-2}. A statistical analysis on nine MEA-type electrodes (Table S1) indicated a lower average V_{oc} value, of 330 mV, for MEA devices that incorporated the Ni–Mo catalyst. These values contrast with the V_{oc} = 600 mV value used in the modeling of the optimal device performance. Significant contributors to the difference include limitations with the Si microwire synthesis and resulting device fidelity. Additionally, the Si-based Ni–Mo/TiO_2 MEA devices suffered from adventitious

Deleted: Figure 7
Formatted: Not Highlight
Deleted: Figure 2
Formatted: Not Highlight
Formatted: Not Highlight
Formatted: Not Highlight
Formatted: Not Highlight

deposition of catalyst and scattering particles on the microwire sidewalls consistent with physisoprtion and/or chemisorption forces that are stronger than the centrifugal force imparted throughout the flocculation process. Deposition of either nanopowder material on the microwire sidewalls acts to reduce the light-limited photocurrent density, as discussed further in the Supporting Information. Each of these performance issues can presumably be addressed with improved attention to growth and processing procedures for Si microwire arrays, providing a credible path to $\eta_{IRC} > 10\%$ for MEA photocathodes.

To illustrate the possibility of improving further the performance of the MEA devices, the origin of the low observed V_{oc} values for devices that incorporated the Ni–Mo catalyst was investigated. Metal incorporation via solid-state reactivity and subsequent diffusion into the Si absorber during the catalyst-activation annealing step likely degrades the minority-carrier lifetime of the Si. Mo concentrations of $<10^{12}$ cm^{-3} can significantly decrease the minority-carrier lifetimes in p-Si.[8,28] Although these low impurity concentrations are difficult to detect analytically, decreases in V_{oc} were observed for Si microwire n^+p-junction samples that contained Ni–Mo particles and were subsequently annealed at 450 °C, as compared to samples from the same substrate that were instead coated with Pt at room temperature (Figure 9). The observed difference in V_{oc} is therefore consistent with a decrease in charge-carrier lifetime due to the presence of impurities in the Si. To remedy this deficiency, carbon-supported Ni–Mo catalysts (Ni–Mo/C) were synthesized without an annealing step following the deposition of the catalyst into the microwire array. Figure 9 demonstrates a recovery of the V_{oc} when Ni–Mo/C catalyst was used without a post-deposition annealing step; however, significant sidewall deposition, due to a reduced efficiency of centrifugal flocculation, precluded these samples from also obtaining exhibiting high J_{ph} values. Further efforts to improve the device fidelity, as well as to optimize the MEA-layer deposition conditions, are warranted to achieve further improvements in the performance of such photocathodes.

Optimization of the Ni-Mo and TiO_2 layer thicknesses could also provide improved performance. Increasing the thickness of the Ni-Mo layer is expected to improve the catalytic activity, but assuming that the TiO_2 thickness remains constant, the reflectivity of the device would increase due to the increase in the height of the Si microwires that protrude from the Ni-Mo/TiO_2 layers. Similarly, an increase in the TiO_2 layer thickness is expected to increase the light scattering until the layer becomes optically dense, at which point the light scattering properties are expected

Formatted: Not Highlight

Formatted: Not Highlight

Deleted: Figure 9

Deleted: Figure 9

Formatted: Not Highlight

to remain relatively constant. However, in an analogous fashion to the effect of increasing the thickness of the Ni-Mo layer, an increase in the thickness of the TiO_2 is expected to increase the device reflectivity by decreasing the Si microwire height that is available for light absorption.

Device Stability: Direct stability measurements were not performed because these Ni-Mo nanopowder electrocatalysts are known to degrade rapidly after ~7 h of operation in acidic conditions consistent with the known chemical instabilities of the individual elements.[5] The device stability is not expected to be limited by Si or TiO_2, as both materials are chemically stable under the operating conditions. Figure S10 and S11 show SEM images after photoelectrochemical testing that confirm that the sample construct remained intact throughout PEC testing, suggesting that the Ni-Mo electrocatalyst under the test conditions will provide the ultimate stability limit for this particular device. Accordingly, mutual compatibility of all components is ultimately desired and thus incorporation of hydrogen-evolution electrocatalysts with long-term stability in acid media should result in improved overall device longevity. The device architecture described herein can accommodate high mass loadings to allow for the use of electrocatalysts that have a relatively low intrinsic catalytic activity, thereby expanding the range of electrocatalyst activity as a trade-off for stability, if needed.

V. CONCLUSIONS

We have designed, fabricated and experimentally verified a broadly applicable photoelectrode architecture that circumvents the trade-off between catalytic activity (*ff*) and optical absorption in the overlayer. This trade-off would otherwise significantly reduce the light-limited photocurrent density (J_{ph}) and, unless mitigated, would preclude efficient solar-driven water splitting. The architecture consists of a high aspect-ratio three-dimensional semiconductor structure (*e.g.* Si microwires) with a particulate catalyst layer covered by a high-dielectric particulate layer that scatters light back into the semiconductor structure. Modeling of the design suggests that $\eta_{IRC} > 10\%$ is possible with earth-abundant electrocatalysts that have a relatively low per-atom activity. The best-performing Si homojunction microwire-array photocathodes investigated herein with ~1–2 mg cm^{-2} of a Ni–Mo nanoparticulate catalyst layer, covered by a TiO_2 nanoparticulate light scattering layer, demonstrated a $\eta_{IRC} = 2.9\%$. Replacing the Ni–Mo nanoparticulate layer with electrolessly deposited Pt on the microwire sidewalls resulted in $\eta_{IRC} = 5\%$, similar to that of the best-performing previously published Si microwire device.[25] The

Formatted: Not Highlight

Formatted: Not Highlight

Formatted: Not Highlight

Formatted: Not Highlight

Formatted: Not Highlight

Formatted: Not Highlight

modeling indicated that still higher η_{IRC} values can be obtained by optimization of the microwire growth and doping process, in conjunction with optimization of the deposition procedures used for the catalyst and optical scattering layers.

VI. ACKNOWLEDGMENTS

Device modeling, fabrication and testing were supported by the Joint Center for Artificial photosynthesis, a DOE Energy Innovation Hub supported through the Office of Science of the U.S. Department of Energy under award number DE-SC004993. Development of the Ni–Mo nanopowder catalyst was supported by the National Science Foundation (NSF) Powering the Planet Center for Chemical Innovation (CHE-1305124) and by the Molecular Materials Research Center of the Beckman Institute at the California Institute of Technology. The authors acknowledge additional support by the Gordon and Betty Moore Foundation (GBMF1225). MRS acknowledges the Resnick Sustainability Institute for a graduate fellowship. JRM acknowledges the Department of Energy, Office of Science, for a graduate research fellowship and the Department of Energy, Office of Energy Efficiency and Renewable Energy, for a SunShot postdoctoral research award.

Figures and Tables

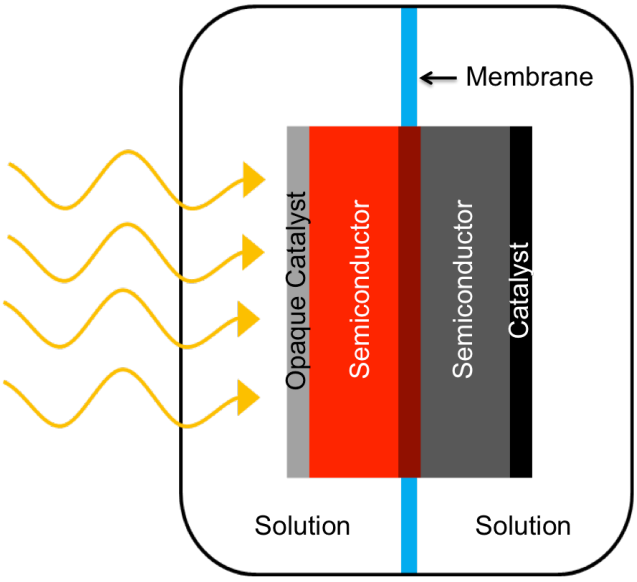

Figure 1: a) Schematic of a water-splitting device incorporating two planar light absorbers in a tandem configuration, two electrocatalysts, and a single tunnel junction to allow serial addition of the photovoltages produced by each semiconducting light-absorber unit. The opaque catalyst on the light-incident surface (left side) is the source of the trade-off between the fill factor (*ff*) and the light-limited current density (J_{ph}).

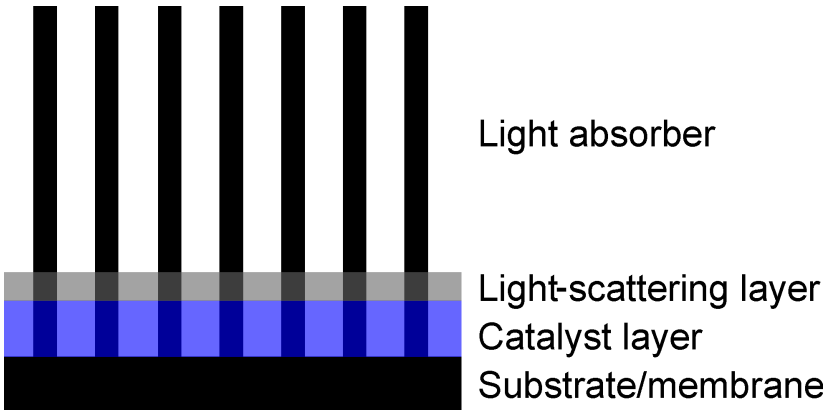

Figure 2: Schematic depiction of the membrane-electrode assembly (MEA)-type hydrogen-evolving photocathode based on arrays of Si microwires embedded in a membrane or supported on a substrate, with a layer of a non-noble catalyst deposited at the base of the array and covered by a light-scattering layer.

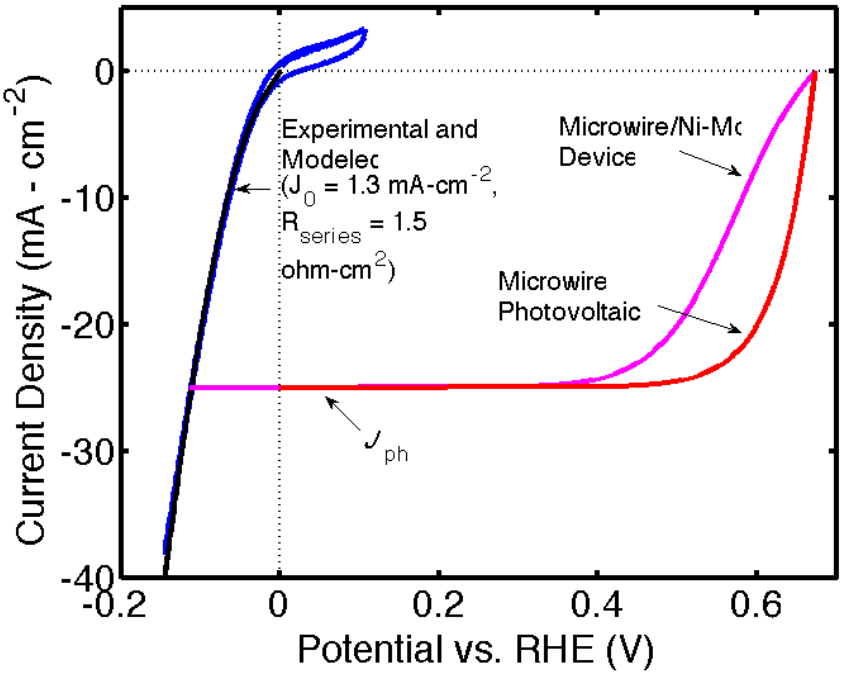

Figure 3: Current-density versus potential (*J-E*) behavior obtained from the modeling of an n^+p-Si microwire-array membrane-electrode assembly (MEA, magenta curve) and for a stand-alone n^+p-Si microwire-array photovoltaic device wired to a discrete, purely catalytic electrode (red curve). Ni-Mo was used as the hydrogen-evolution catalyst in both cases, and the dark catalytic activity of the catalyst was modeled according to experimental observations (blue curve).

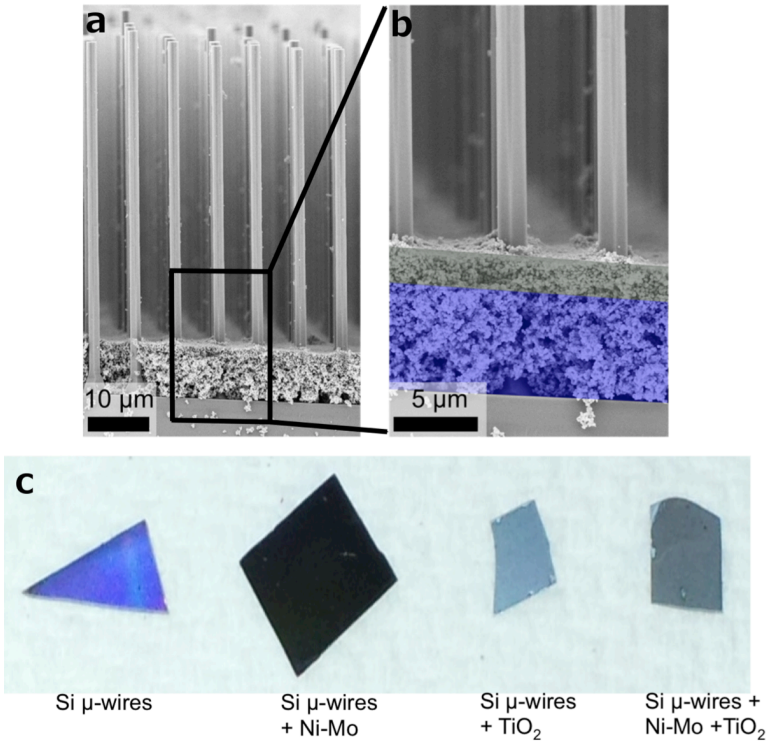

Figure 4: a) Scanning-electron micrographs of a silicon microwire array onto which a layer of Ni–Mo nanopowder and a layer of TiO_2 light-scattering particles have been deposited sequentially. b) Detail of the boxed area in a, highlighted to delineate the Ni-Mo nanopowder layer beneath the layer of TiO_2 particles. c) Optical image of four microwire arrays with different nanoparticulate depositions within the array.

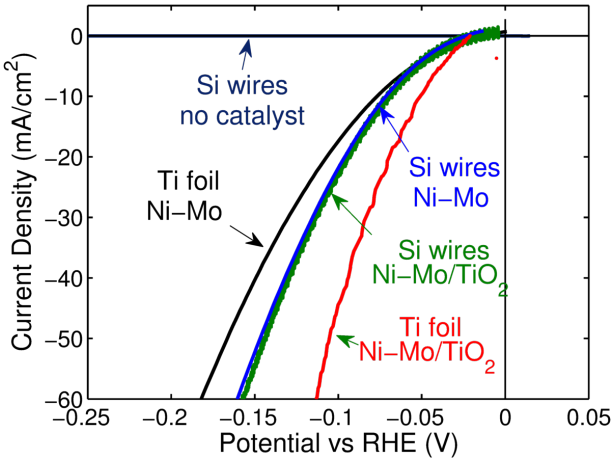

Figure 5: Dark *J-E* behavior for electrodes with the noted compositions. The Si microwire samples were degenerately doped p-type and were metallized with Ag to minimize the interfacial contact resistance. All of the samples were evaluated in 1.0 M H_2SO_4(aq), and Ni–Mo samples had mass loadings of ~1 mg cm^{-2}, except for the Ti foil Ni–Mo/TiO_2 sample which had a mass loading of ~3 mg cm^{-2}.

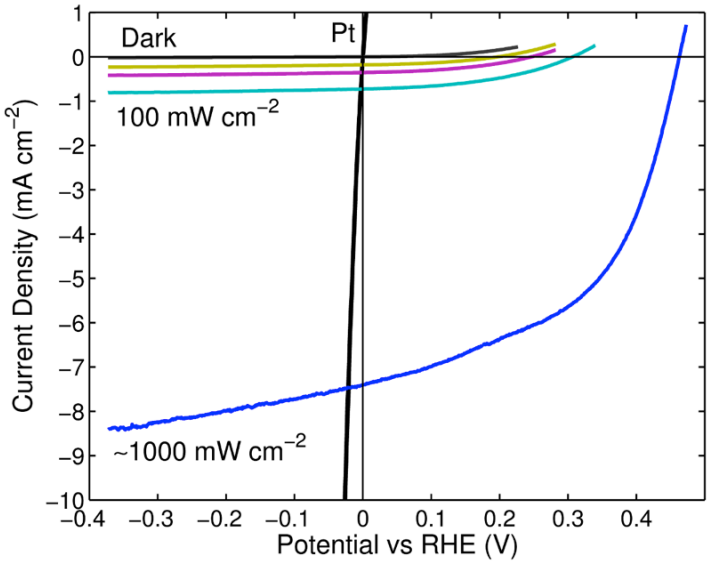

Figure 6: Current-density versus potential (*J*-*E*) behavior of a planar n^+p-Si/Ni–Mo/TiO_2 photocathode in contact with 0.5 M H_2SO_4(aq) over a range of illumination intensities from dark to ~10 Suns, with the light having an AM 1.5G simulated spectral distribution. A polished Pt button control electrode is shown for reference.

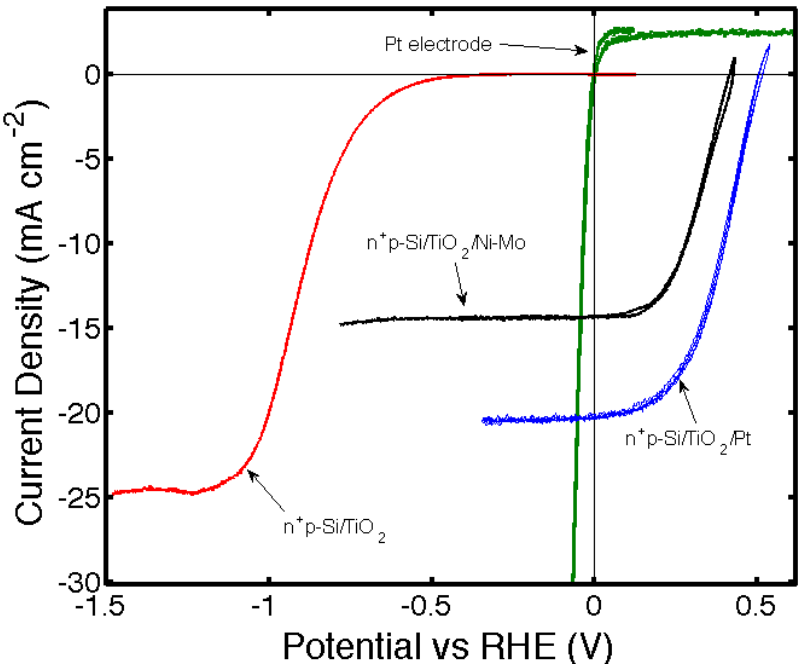

Figure 7: Current-density versus potential (*J-E*) behavior of the best-performing Si microwire-array devices prepared in this work, as well as for control samples involving Si microwires without the catalyst (n^+p-Si/TiO_2) and instead utilizing only a Pt electrode in the dark.

Formatted: Not Highlight

Formatted: Not Highlight

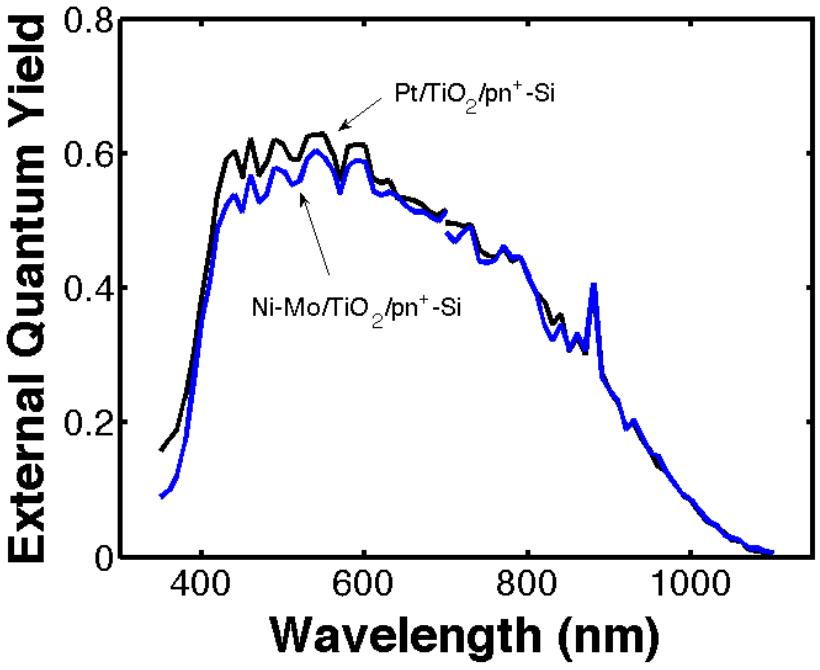

Figure 8: Spectral response data for the best-performing n^+p-Si microwire-array photocathode loaded with Ni–Mo and TiO_2 scattering particles (blue curve) and for the best-performing n^+p-Si microwire-array photocathode loaded with Pt and TiO_2 scattering particles (black curve). Integration of each data set with the AM 1.5G spectrum binned at the same intervals (50 nm) resulted in light-limited photocurrent densities of 15.8 and 17.5 mA cm^{-2} for the Ni–Mo and Pt samples, respectively. The slightly lower integrated current density than the J_{sc} measured for the Pt sample could be due to morphological changes in the Pt between the *J-E* and spectral response measurements (>1 month).

Formatted: Not Highlight

Formatted: Not Highlight

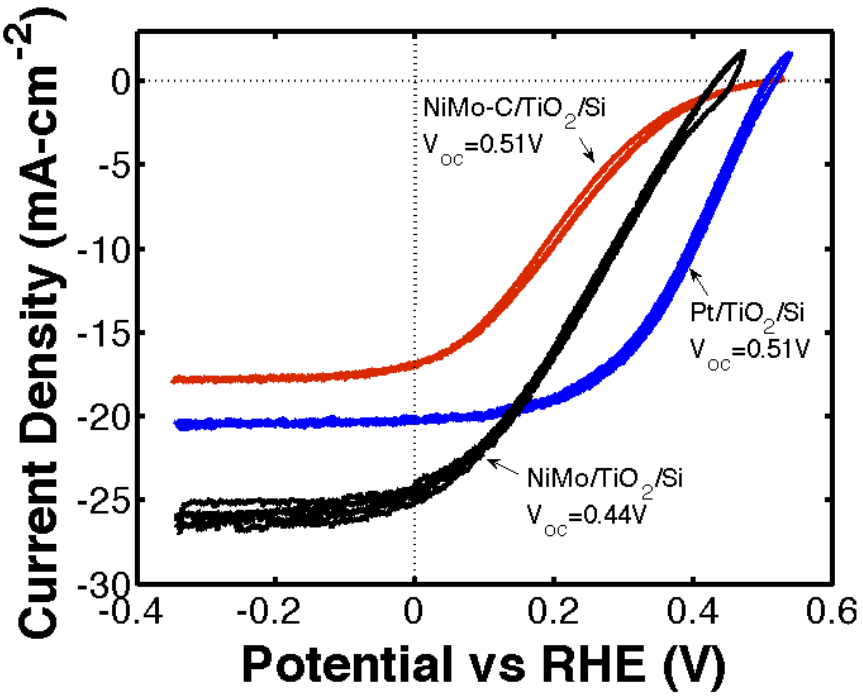

Figure 9: Current-density versus potential (*J-E*) behavior for three samples in 1.0 M H_2SO_4(aq), demonstrating the decrease in open-circuit voltage (V_{oc}) consistently observed in the Ni–Mo containing samples as compared to in samples that were coated with Pt. A V_{oc} similar to that exhibited by the Pt-coated Si microwire arrays was observed upon introduction of a carbon-supported Ni-Mo catalyst that did not require annealing to activate the Ni-Mo after deposition.

Table 1: Figures of merit for the best-performing Si microwire devices of each type prepared herein as determined from *J-E* behavior.

Device	V_{oc} (mV)	J_{sc} (mA cm^{-2})	*ff*	η_{IRC} (%)
TiO_2 layer	n/a	25	0	0
TiO_2/Pt	510	20.2	0.49	5
TiO_2/Ni–Mo	420	14.3	0.48	2.9

Formatted: Not Highlight

Formatted: Not Highlight

Formatted: Not Highlight

Notes and References

1. E. L. Warren, J. R. McKone, H. A. Atwater, H. B. Gray, and N. S. Lewis, *Energy & Environmental Science*, 2012, **5**, 9653.
2. J. R. McKone, S. C. Marinescu, B. S. Brunschwig, J. R. Winkler, and H. B. Gray, *Chem. Sci.*, 2014, **5**, 865.
3. M. R. Shaner, H. A. Atwater, and N. S. Lewis, 2012.
4. A. Heller, D. E. Aspnes, J. D. Porter, T. T. Sheng, and R. G. Vadimsky, *J. Phys. Chem.*, 1985, **89**, 4444–4452.
5. J. R. McKone, B. F. Sadtler, C. A. Werlang, N. S. Lewis, and H. B. Gray, *ACS Catal.*, 2013, **3**, 166–169.
6. E. J. Popczun, C. G. Read, C. W. Roske, N. S. Lewis, and R. E. Schaak, *Angewandte Chemie International Edition*, 2014, **53**, 5427–5430.
7. E. J. Popczun, J. R. McKone, C. G. Read, A. J. Biacchi, A. M. Wiltrout, N. S. Lewis, and R. E. Schaak, *J. Am. Chem. Soc.*, 2013, **135**, 9267–9270.
8. M. D. Kelzenberg, S. W. Boettcher, J. A. Petykiewicz, D. B. Turner-Evans, M. C. Putnam, E. L. Warren, J. M. Spurgeon, R. M. Briggs, N. S. Lewis, and H. A. Atwater, *Nature Materials*, 2010, **9**, 239–244.
9. L. Trotochaud, T. J. Mills, and S. W. Boettcher, *J. Phys. Chem. Lett.*, 2013, **4**, 931–935.
10. A. C. Nielander, M. R. Shaner, K. M. Papadantonakis, S. A. Francis, and N. S. Lewis, *Energy & Environmental Science*, 2015.
11. S. Licht, B. Wang, S. Mukerji, T. Soga, M. Umeno, and H. Tributsch, *Journal of Physical Chemistry B*, 2000, **104**, 8920–8924.
12. J. A. Seabold and K.-S. Choi, *J. Am. Chem. Soc.*, 2012, **134**, 2186–2192.
13. Y. Chen, K. Sun, H. Audesirk, C. Xiang, and N. S. Lewis, *Energy & Environmental Science*.
14. B. M. Kayes, H. A. Atwater, and N. S. Lewis, *J. Appl. Phys.*, 2005, **97**, 114302.
15. J. R. Maiolo, B. M. Kayes, M. A. Filler, M. C. Putnam, M. D. Kelzenberg, H. A. Atwater, and N. S. Lewis, *J. Am. Chem. Soc.*, 2007, **129**, 12346–12347.
16. A. P. Goodey, S. M. Eichfeld, K.-K. Lew, J. M. Redwing, and T. E. Mallouk, *J. Am. Chem. Soc.*, 2007, **129**, 12344–12345.
17. G. Yuan, H. Zhao, X. Liu, Z. S. Hasanali, Y. Zou, A. Levine, and D. Wang, *Angewandte Chemie International Edition*, 2009, **48**, 9680–9684.
18. T. F. Jaramillo, K. P. Jorgensen, J. Bonde, J. H. Nielsen, S. Horch, and I. Chorkendorff, *Science*, 2007, **317**, 100–102.
19. C. W. Roske, E. J. Popczun, B. Seger, C. G. Read, T. Pedersen, O. Hansen, P. C. K. Vesborg, B. S. Brunschwig, R. E. Schaak, I. Chorkendorff, H. B. Gray, and N. S. Lewis, *J. Phys. Chem. Lett.*
20. M. C. Putnam, S. W. Boettcher, M. D. Kelzenberg, D. B. Turner-Evans, J. M. Spurgeon, E. L. Warren, R. M. Briggs, N. S. Lewis, and H. A. Atwater, *Energy & Environmental Science*, 2010, **3**, 1037.
21. M. R. Shaner, K. T. Fountaine, and H.-J. Lewerenz, *Appl. Phys. Lett.*, 2013, **103**, 143905.
22. S. W. Boettcher, J. M. Spurgeon, M. C. Putnam, E. L. Warren, D. B. Turner-Evans, M. D. Kelzenberg, J. R. Maiolo, H. A. Atwater, and N. S. Lewis, *Science*, 2010, **327**, 185–187.
23. R. H. Coridan, A. C. Nielander, S. A. Francis, M. T. McDowell, V. Dix, S. M. Chatman, and N. S. Lewis, *Energy & Environmental Science*.
24. V. Mehta and J. S. Cooper, *Journal of Power Sources*, 2003, **114**, 32–53.

25. S. W. Boettcher, E. L. Warren, M. C. Putnam, E. A. Santori, D. Turner-Evans, M. D. Kelzenberg, M. G. Walter, J. R. McKone, B. S. Brunschwig, H. A. Atwater, and N. S. Lewis, *J. Am. Chem. Soc.*, 2011, **133**, 1216–1219.
26. E. Aharon-Shalom and A. Heller, *J Electrochem Soc*, 1982, **129**, 2865–2866.
27. C. Xiang, A. C. Meng, and N. S. Lewis, *Proceedings of the National Academy of Sciences*, 2012, **109**, 15622–15627.
28. J. R. J. Davis, A. Rohatgi, R. H. Hopkins, P. D. Blais, P. Rai-Choudhury, J. R. McCormick, and H. C. Mollenkopf, *Electron Devices, IEEE Transactions on*, 1980, **27**, 677–687.

Supplementary Information Available

Electronic Supplementary Information (ESI), including complete materials and methods, Figures S1-S8 and associated discussion, are available.